JOURNAL OF SOLID STATE CHEMISTRY **137,** 33–41 (1998)
ARTICLE NO. SC977672

The Vibrational Spectra and Decomposition of α-Calcium Nitride (α-Ca_3N_2) and Magnesium Nitride (Mg_3N_2)

Anton M. Heyns[1] and Linda C. Prinsloo

Institute of Applied Materials, University of Pretoria, 0002 Pretoria, South Africa

and

Klaus-Jürgen Range and Martin Stassen

Institute of Inorganic Chemistry, University of Regensburg, D-8400 Regensburg, Germany

Received July 7, 1997; accepted October 23, 1997

α-Ca_3N_2 has been characterized by X-ray powder diffraction and its structure confirmed by a crystal structure refinement with the Rietveld method. Ca_3N_2 and the isostructural Mg_3N_2 crystallize in the anti-bixbyite structure of the mineral $(Mn, Fe)_2O_3$ in the body-centered space group of $Ia3(T_h^7)$, and the general appearance of their infrared and Raman spectra resembles that of the sesquioxides belonging to the same space group. The decomposition of M_3N_2 (M = α-Ca, Mg) into $M(OH)_2$ and NH_3, when exposed to the atmosphere, is reported. The presence of NH_4^+ vibrational bands in the decomposition products is explained in terms of the existence of Brønsted acid centers on the surface of the solid. During the initial stages of decomposition, infrared bands characteristic of adsorbed NH_3 were observed, showing that Lewis centers also exist on the surface. The decomposition product $Mg(OH)_2$ has weaker proton-donating centers than $Ca(OH)_2$. The kinetics of the decomposition of Mg_3N_2, which is a much slower reaction than that of α-Ca_3N_2, has been studied with FT-IR microspectrometry, and it is shown that the formation of $Mg(OH)_2$ is a three-dimensional diffusion process while the proton donation by the hydroxide to adsorbed NH_3 to form NH_4^+ ions is a quasi-first-order reaction.

INTRODUCTION

Calcium nitride is a salt-like nitride, and its properties have been reported extensively in the literature (1–5). It exists in various modifications, viz. α-Ca_3N_2 (reddish-brown) (2), β-Ca_3N_2 (black) (6), γ-Ca_3N_2 (yellow) (7), and a high-pressure phase (yellow) (8). α-Ca_3N_2 is unusual in the sense that the calcium ions have the very low coordination number of 4 (1). This compound has been used as a catalyst for the phase transition in BN under high pressures (5), particularly since the crystal structures of the two nitrides show a close resemblance. It is further well known that α-Ca_3N_2 is very sensitive with respect to moisture, and it is therefore important to study the decomposition of this compound. Mg_3N_2 and α-Ca_3N_2 are isostructural (9), and it is of interest to compare these compounds with respect to their vibrational spectra and decomposition to learn more about the bonding in and the solid state reactions of these two nitrides.

In the present study, the crystal structure of α-Ca_3N_2 is further investigated by means of X-ray powder diffraction using the Rietveld method, and the infrared and Raman spectra have been obtained of both α-Ca_3N_2 and Mg_3N_2. Some infrared spectra of salt-like nitrides were published (10), but we could not find any references to the Raman spectra of these materials. In this paper, the decomposition products of both compounds, when exposed to the air, have been studied with infrared and Raman methods, and the decomposition reaction of Mg_3N_2, which is much slower than that of α-Ca_3N_2, has been followed with time using FT-IR microspectrometry.

EXPERIMENTAL

α-Ca_3N_2 and Mg_3N_2 were obtained from Alfa Co. Ltd., with stated purities of 99% and 99.5%, respectively. α-Ca_3N_2 was ground into a fine powder in a glovebox and placed in a quartz ampule which was sealed under vacuum. The ampule was heated in a muffle oven at 700°C for 1 day. Some of the powder was then transferred to a capillary tube, and the X-ray powder diffraction of the compound was obtained using a STADI P automatic powder diffractometer from the company STOE in Darmstadt, Germany.

[1]To whom correspondence should be addressed.

0022-4596/98 $25.00

For the Raman measurements, the samples were sealed in capillary tubes under vacuum and the spectra were measured using an $X-Y$ Dilor Raman spectrometer with a $100\times$ objective of a microprobe attached to the instrument. The 514.5 nm line of an Ar^+ ion laser, Innova Model 305, obtained from Coherent Radiation was used to excite the spectra. The Raman spectra were also obtained of samples in the bulk mode. The spectral resolution was $2.0\,cm^{-1}$ in all the spectra. Samples of α-Ca_3N_2 and Mg_3N_2 were pressed into KBr or polyethylene pellets for the mid- and far-infrared spectra, respectively. The infrared spectra were obtained using a Bruker 113 V FT-IR spectrometer at a resolution of $2\,cm^{-1}$ in the spectral range 50–4000 cm^{-1}. The decomposition reaction of Mg_3N_2 was followed with time in situ, using infrared microspectroscopy. These spectra were recorded with a Bruker A590 infrared microscope in the transmission mode, attached to the 113V spectrometer. The spectral range of the microscope is 600–4000 cm^{-1}; a liquid nitrogen cooled MgCdTe detector was used, and 32 scans were taken for each recording with a spectral resolution of $4\,cm^{-1}$. The experiment was repeated four times. The decomposition reaction of α-Ca_3N_2, ground into a finely divided powder (< 0.04 mm), proceeded too rapidly to follow with the present experimental procedure. The size of the particles of both of these nitrides is an important factor in determining the rate of the reaction, very clearly demonstrating the fact that it is a surface reaction and therefore dependent on the surface area.

STRUCTURAL DETAILS AND VIBRATIONAL SELECTION RULES

Structures for α-Ca_3N_2 have been proposed from earlier powder diffraction data (3), and a single-crystal X-ray study of this compound has also been undertaken (4). It belongs to the space group $Ia3$ (No. 206), $Z = 16$, and has the antibixbyite structure. In the present study, the powder diffraction data were recorded on a two-circle powder diffractometer and Rietveld refinement was used to obtain the exact structural parameters. The atomic coordinates obtained in the present study are listed in Table 1, and the lattice parameters and atomic coordinates of various studies are compared in Table 2. The bond angles and lengths, which appear in subsequent figures, were calculated from our own data; however, it is also evident from Table 2 that the results of the different studies agree rather well.

TABLE 1
Atomic Coordinates in α-Ca_3N_2

Atoms	Wyckoff notation	Atomic coordinates x/a	y/b	z/c	U_{iso} (Å^2)
Ca	48e	0.392(1)	0.155(1)	0.381(1)	0.0001
N(1)	8b	1/4	1/4	1/4	0.0001
N(2)	24d	0.956(3)	0	1/4	0.0001

TABLE 2
A Comparison of the Lattice Constants and Atomic Positions in α-Ca_3N_2 Obtained in Various Studies

Reference	a (Å)	Atomic coordinates x(N(2))	x(Ca)	y(Ca)	z(Ca)
This study	11.467(1)	0.956(3)	0.392(1)	0.155(1)	0.381(1)
Y. Laurent *et al.* (3)	11.473(1)	0.960(2)	0.389(1)	0.153(1)	0.382(1)
P. Höhn (4)	11.474(2)	0.960(2)	0.39011(5)	0.15394(4)	0.38244(5)

The fourfold coordination of the calcium ions is shown in Fig. 1 and it is clear that it can be described as a distorted tetrahedral configuration. The N(1) ions are surrounded by six Ca^{2+} ions in a distorted octahedral configuration, as can be seen in Fig. 2. The N(2) ions are surrounded by six Ca^{2+} ions in a distorted trigonal prismatic configuration, as can be seen in Fig. 3.

Further structural details have been published, particularly as far as the values of the bond angles are concerned (11), and they will not be repeated here. The isostructural Mg_3N_2 has a lattice parameter of 9.964 Å and the following

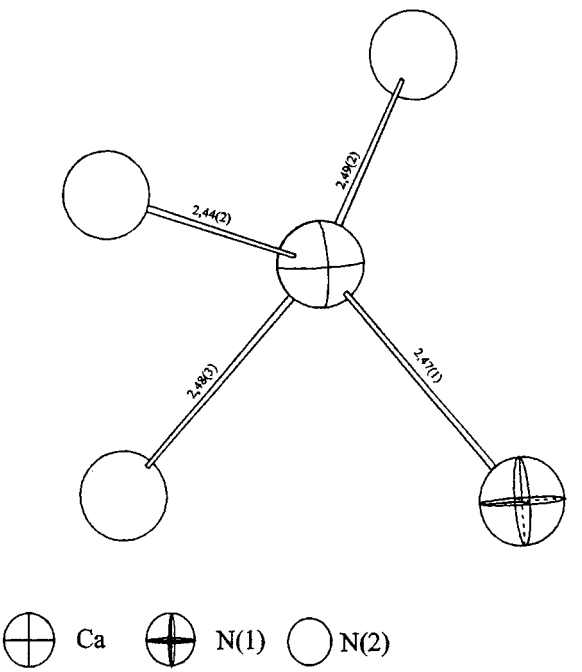

FIG. 1. The distorted tetrahedral coordination of the calcium ions in α-Ca_3N_2.

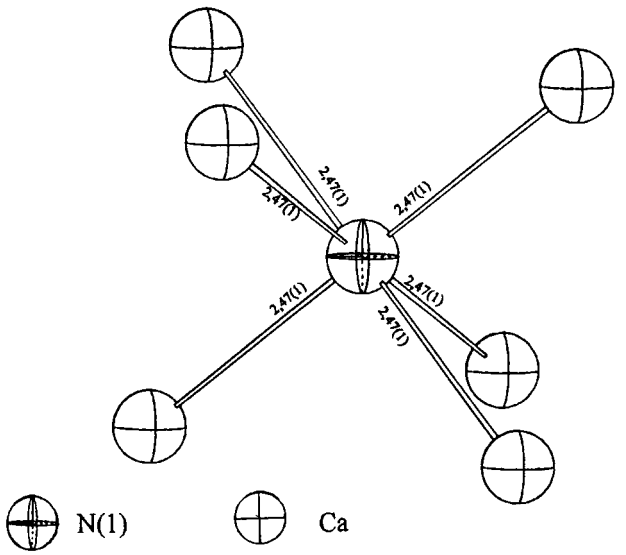

FIG. 2. The distorted octahedral coordination of the N(1) ions in α-Ca_3N_2.

atomic coordinates: Mg, 0.387x, 0.152y, 0.382z; N(1), $\frac{1}{4}x$, $\frac{1}{4}y$; $\frac{1}{4}z$; N(2), 0.963x; O; $\frac{1}{4}z$ (9).

The vibrations that can be expected to occur in this type of anti-bixbyite structure have already been published (12). The distribution among the different representations of T_h^7 symmetry is as follows: $\Gamma_{\text{Total}} = 4A_g(R) + 4E_g(R) + 14F_g(R) + 5A_u(-) + 5E_u(-) + 16F_u(IR)$. Accordingly, the Raman spectra of these nitrides are expected to display more features than the infrared spectra. It is shown in Fig. 1 that each Ca^{2+} ion is bonded to one N(1) ion and three N(2) ions, the latter being of different bond lengths. There are consequently 24 Ca–N(1) bonds in the primitive unit cell of α-Ca_3N_2 (N(1) is surrounded by six Ca^{2+} ions) and 24 Ca–N(2) bonds for each of the 2.48, 2.49 Å and 2.44 Å bond lengths. A large number of Ca–N stretching modes can therefore occur in the vibrational spectra of α-Ca_3N_2, viz. $\Gamma_{\text{stretch}} = 4A_g + 4E_g + 12F_g + 4A_u(-) + 4E_u(-) + 12F_u(IR)$ (13). However, if one considers that the different bond lengths in α-Ca_3N_2 are not widely different, except perhaps for the value of 2.44 Å for Ca–N(2), it will be unrealistic to expect a resolution of all the possible modes in the vibrational spectra recorded of powdered solids.

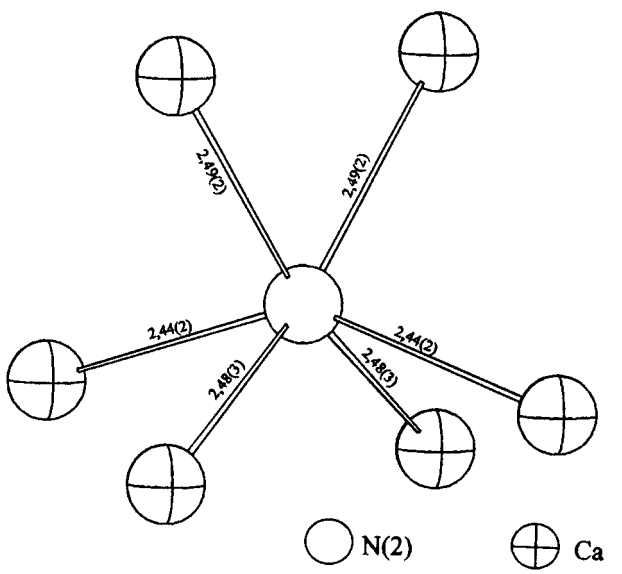

FIG. 3. The distorted trigonal prismatic coordination of the N(2) ions in α-Ca_3N_2.

VIBRATIONAL SPECTRA

The Raman spectra of α-Ca_3N_2 and Mg_3N_2 are shown in Fig. 4, the infrared spectra are shown in Fig. 5, and these results are summarized in Table 3.

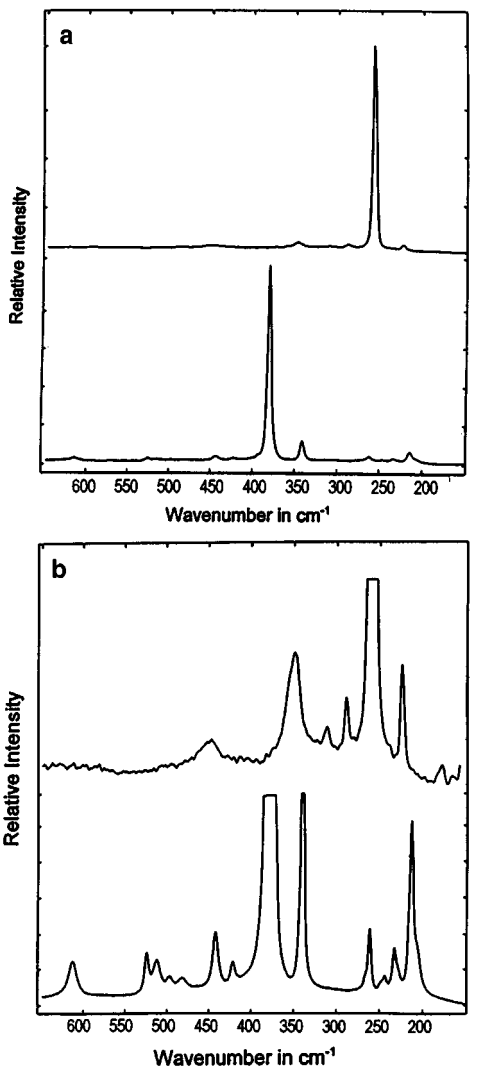

FIG. 4. (a) The Raman spectra of α-Ca_3N_2 (top) and Mg_3N_2 (bottom). (b) The same spectra recorded using longer integration times.

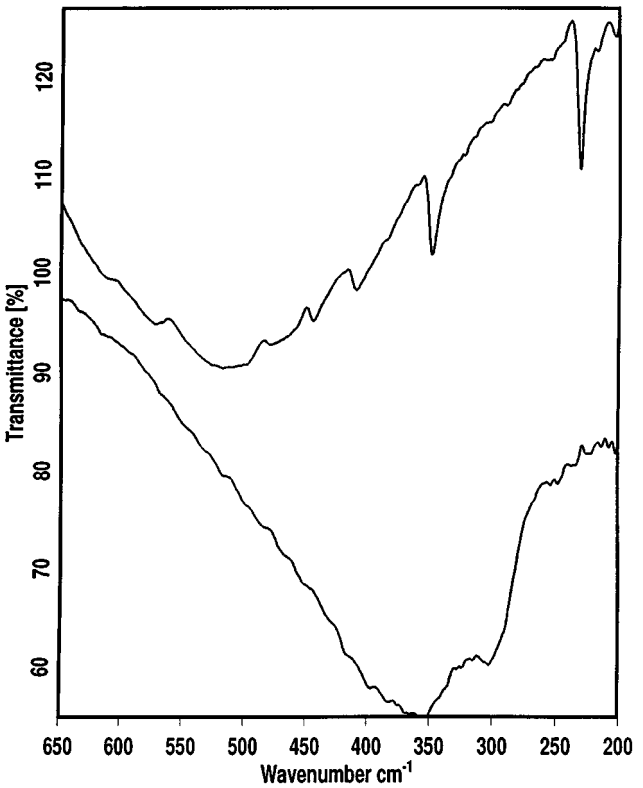

FIG. 5. The infrared spectra of Mg_3N_2 (top) and α-Ca_3N_2 (bottom) in the wavenumber range of 200–650 cm^{-1}.

As can be seen in Fig. 5, the infrared spectrum of α-Ca_3N_2 has broad, intense features at 353 and 302 cm^{-1}, and the broadness of these peaks, weak shoulders and asymmetries that are not well resolved, suggest an undetermined number of components in this wavenumber range. The Raman spectrum shows bands at 350, 311, and 289 cm^{-1} in this wavenumber range. These bands are most probably asymmetric stretching modes since they are very weak in the Raman spectra and strong in the infrared spectra. In Mg_3N_2, these modes are better resolved and at least six components can be identified in the infrared spectrum between 410 and 610 cm^{-1} (Table 3, Fig. 5) and seven Raman bands between 420 and 612 cm^{-1} (Table 3, Fig. 4). It is obvious that a detailed assignment of the bands cannot be made at this stage, but it must be noted that the general pattern of these spectra very much resembles that of the isostructural sesquioxides (12).

It is evident from Fig. 4 that the Raman spectra are dominated by intense modes at 258 cm^{-1} in α-Ca_3N_2 and at 379 cm^{-1} in Mg_3N_2. These intense peaks, as well as their much weaker components at 225 and 338 cm^{-1} in α-Ca_3N_2 and Mg_3N_2, respectively, do not have counterparts in the infrared spectra at exactly the same wavenumbers (although in Mg_3N_2, the well-characterized peak in the infrared spectrum at 350 cm^{-1} could be such a candidate). It is obvious

TABLE 3
Infrared and Raman Bands (in cm^{-1}) of α-Ca_3N_2 and Mg_3N_2 [a]

α-Ca_3N_2		Mg_3N_2	
IR	Raman	IR	Raman
—	—	610 sh	612 vw
—	—	572 s	—
—	− 350 vw	—	525 vw
~353 vs	311 vw	~518 vs	512 vw
—	—	—	496 vw
—	—	479 vs	481 vw
—	289 vw	445 s	442 vw
—	—	410 s	420 vw
—	258 vs	—	379 vs
—	225 w	—	338 m
~302 vs	—	350 s	—
—	—	—	260 vw
—	—	—	243 vw
—	—	232 s	232 vw
—	—	204 w	213 vw

[a] *Key*: vs = very strong, s = strong, m = medium, w = weak, vw = very weak, sh = shoulder.

that the most intense modes in the Raman spectra must be the totally symmetric metal–nitride vibrations. A dominant Raman peak has also been observed in the spectra of all the sesquioxides with the anti-bixbyite structure and has been assigned to the metal–oxygen symmetric stretching mode (12). It may be possible to assign the modes occurring at lower wavenumbers in both the infrared and Raman spectra to bending vibrations.

In the study of the sesquioxides of the rare earths (12), it was shown that the highest frequency infrared band varies linearly with the metal–oxygen distance and some correlation also exists between the highest frequency Raman band and the highest intensity Raman band and the metal–oxygen distance. The ratio of the most intense infrared bands in α-Ca_3N_2 and Mg_3N_2 is equal to $353/518 = 0.68$, which is exactly equal to the ratio of the most intense Raman bands in the two compounds, viz. $258/379 = 0.68$. The square root of the masses of the two metal ions is equal to 0.78, and it is clear that the shift in the wavenumbers of these modes from α-Ca_3N_2 to Mg_2N_2 cannot be due to a mass effect only. The smaller ionic radius of Mg^{2+} with respect to Ca^{2+} must give rise to a higher lattice energy for Mg_3N_2 than for the isostructural α-Ca_3N_2, and this is clearly reflected by the wavenumbers at which these stretching modes occur. The Mg–N bonds of 2.13 Å are also considerably shorter than the average value of 2.47 for Ca–N in α-Ca_3N_2.

DECOMPOSITION OF α-Ca_3N_2 AND Mg_3N_2

It can be expected that α-Ca_3N_2 and Mg_3N_2, in contact with moisture from the atmosphere, will decompose as

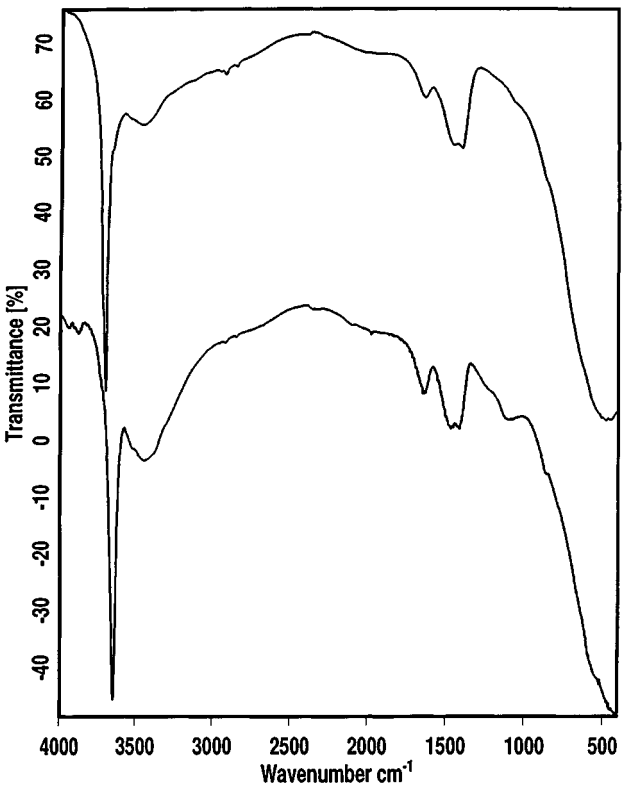

FIG. 6. The midinfrared spectra of decomposed Mg_3N_2 (top) and α-Ca_3N_2 (bottom).

follows:

$$M_3N_2(s) + 6H_2O(g) \rightarrow 3M(OH)_2(s) + 2NH_3(g)$$

$$(M = Ca, Mg).$$

The infrared spectra of partially decomposed α-Ca_3N_2 and Mg_3N_2 are shown in Fig. 6, and the Raman spectra of the former are shown in Fig. 7. These results are summarized in Table 4.

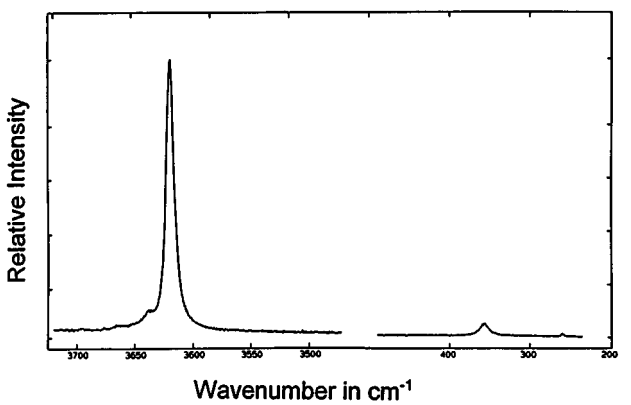

FIG. 7. The Raman spectrum of decomposed α-Ca_3N_2.

The infrared and Raman bands of $Ca(OH)_2$ and $Mg(OH)_2$ (14) are also shown in Table 4, and it is clear from the occurrence of ν_{OH} at 3642 cm^{-1} in the infrared spectrum of decomposed α-Ca_3N_2 and at 3620 cm^{-1} in the Raman spectrum of the same product that the main decomposition product is indeed $Ca(OH)_2$. The same applies to decomposed Mg_3N_2 where ν_{OH} has been observed at 3697 cm^{-1} in the infrared and at 3652 cm^{-1} in the Raman spectrum. However, a closer scrutiny of the spectra in Fig. 6 reveals the presence of a large number of features which do not belong to either M_3N_2 or $M(OH)_2$ (M = Ca, Mg) and which must therefore be assigned to the other reaction product NH_3(g). The Raman spectra did not reveal these features to the same extent as infrared spectroscopy, and the latter method is of course a classical one for the detection of Brønsted and Lewis centers on the surface of a solid when gaseous ammonia is adsorbed (15). The criterion for determining the presence of these centers is the detection of ammonium ions for Brønsted centers and coordinated ammonia on Lewis centers (15). The infrared and Raman spectra of gaseous NH_3, solid NH_3, coordinated NH_3, and solid NH_4^+ are summarized in Table 5.

Gaseous NH_3 has four fundamental vibrational modes under C_{3v} symmetry for the "free" NH_3 molecule. The totally symmetric bending mode ν_2 can be split into two bands because of inverse doubling and is sensitive to the environment. Formation of a coordination bond between NH_3 and a cation complex-forming agent leads to radical changes in the character of its vibrations. The formation of a coordination band enhances the force constant and consequently the wavenumbers of ν_2. The wavenumber of ν_4, the asymmetric NH_3 bending mode, is the least sensitive to the charge and nature of the metal.

If gaseous NH_3 is adsorbed on to the surface of a solid hydroxide, a hydrogen bond is formed between the N atom and the surface hydroxyl group (H_3N---H–O) and if the centers on the surface of the hydroxide are capable of protonating the adsorbed ammonia molecules, ammonium ions are yielded. Two distinct infrared-active modes of the NH_4^+ ions occur at 3145 and 1400 cm^{-1}, and they can be assigned to the asymmetric stretching and bending modes ν_3 and ν_4, respectively, which are both of F_2 symmetry under T_d symmetry. Two Raman-active modes occur at 3040 and 1680 cm^{-1}, and they can be assigned to ν_1 and ν_2 modes which are of A_1 and E symmetry, respectively. Upon lowering the symmetry, for example to C_{3v} when H_3N---H---O is formed, all the Raman-active modes are infrared-active and vice versa; however, it can be expected that primarily two infrared-active NH_4^+ modes will be observed, viz. ν_3 and ν_4, although the ν_2 band of NH_4^+ has also been observed at $\sim$1690 cm^{-1} in some of these spectra (15). The splitting of ν_4 into two or three components can be a useful criterion to determine the symmetry of the (H_3N–H^+---O^{-2}) entity. If two components of $\nu_4(NH_4^+)$ are

TABLE 4
Infrared and Raman Bands (in cm^{-1}) of $Ca(OH)_2$ and $Mg(OH)_2$ Compared with Those of the Decomposition Products of α-Ca_3N_2 and Mg_3N_2 [a]

$CaOH_2$ (14)		Decomposition product of α-Ca_3N_2		$Mg(OH)_2$ (14)		Decomposition product of Mg_3N_2		
IR	Raman	IR	Raman	IR	Raman	IR	Raman	Assignment
—	—	3930 vw	—	—	—	—	—	?
—	—	3870 vw	—	—	—	—	—	?
—	—	—	—	—	—	—	3738 vw	
—	—	3691 m	3638 w	—	—	3711 w	3674 w	ν_{OH}
—	—	—	—	—	—	—	3712 w	ν_{OH}
3640	—	3642 vs	—	− 3688	—	3697 vs	—	ν_{OH}-A_{2u}
—	3620	—	3620 vs	—	− 3652 vs	—	3652 vs	ν_{OH}-A_{1g}
—	—	~3456	—	—	—	~3442	—	$\nu_4(NH_4^+ + NH_3)$
—	—	—	—	—	—	—	3300 w	$\nu_3(NH_4^+ + NH_3)$
—	—	2926 vw	—	—	—	2926 vw	—	—
—	—	2854 vw	—	—	—	2854 vw	—	—
—	—	~2120 w	—	—	—	—	—	—
—	—	—	—	—	—	2035 vw	—	—
—	—	1986 w	—	—	—	1981 w	—	—
—	—	1641 m	—	—	—	1653 m	—	$\nu_4(NH_3)$
—	—	1459 m	—	—	—	1472 m	—	$\nu_4(NH_4^+)$
—	—	1406 m	—	—	—	1419 m	—	$\nu_4(NH_4^+)$
—	—	~1224	—	—	—	—	—	—
—	—	1129	—	—	—	—	—	—
—	—	—	1080–1100 w	—	—	—	1080 w	$\nu_2(NH_3)$
—	—	879 w	—	—	725	—	—	—
—	680	—	686	—	—	—	—	ν(R)-E_g
334	—	—	—	461	—	—	—	ν(T)-A_{2u}
—	357 w	—	357 w	—	443 w	—	441 w	ν(T)-A_{1g}
373	—	~375 w	—	416 w	—	—	—	ν(R)-E_u
288	—	~290 w	—	361	—	—	—	ν(T)-E_u
—	254	—	258	—	280	—	277	ν(T)-E_g

[a] The vibrational bands and assignment in Ref. (14) were used for both $Mg(OH)_2$ and $Ca(OH)_2$.

observed, as well as one absorption peak representing $\nu_2(NH_4^+)$, the symmetry of the hydrogen-bonded complex is C_{3v}. If $\nu_4(NH_4^+)$ is split into three components, the symmetry is C_{2v} (or lower) and indicates the presence of two hydrogen bonds between the ion and the surface (15).

Being so insensitive to the environment, the asymmetric bending mode (ν_4) of ammonia is very difficult to separate from that of ν_2 of NH_4^+ because they both occur in the wavenumber range of 1640–1700 cm^{-1} (15). If both physisorbed and chemisorbed NH_3 species are present on the surface of a solid, the bands occurring in this wavenumber range cannot be used as criteria to draw any conclusions regarding the concentrations and properties of these species. To separate chemisorbed from physisorbed NH_3, the latter is usually outgassed at elevated temperatures so that only chemisorbed NH_3 remains on the surface of the solid (15).

TABLE 5
Vibrational Bands of Gaseous, Solid, and Coordinated NH_3 and NH_4^+ Ions (15)

Species	ν_1-stretch	ν_2 bend	ν_3 stretch	ν_4 bend
NH_3(gas)	3336	968–932	3444	1628
NH_3(solid)	3223	1060	3378	1646
NH_3 in amino complexes	3115–3330	1170–1361	3200–3412	1550–1655
NH_4^+ [a]	3040 (R)	1680 (R)	3145 (IR)	1400 (IR)

[a] R, Raman active; IR, infrared active.

The infrared spectra of decomposed α-Ca_3N_2 and Mg_3N_2 can now be analyzed in the light of the abovementioned facts. With decomposition of these nitrides, NH_3(g) will be formed and will diffuse to the surface of the sample where it will be physisorbed and then chemisorbed as a result of the protonation of the NH_3 groups by the OH ones. Brønsted acid centers with hydroxy groups with sufficiently mobile protons will form on the surface of the compounds as a result of the decomposition reaction and NH_4^+ ions will be formed. This process is demonstrated in Fig. 8 showing the decomposition of Mg_3N_2 followed under the infrared

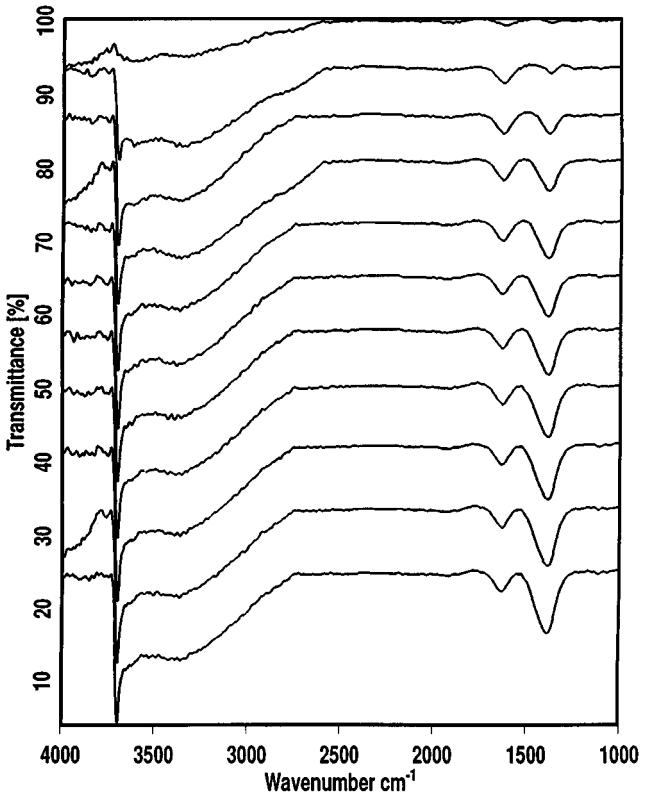

FIG. 8. The decomposition of Mg_3N_2 followed with time with FT-IR microspectroscopy.

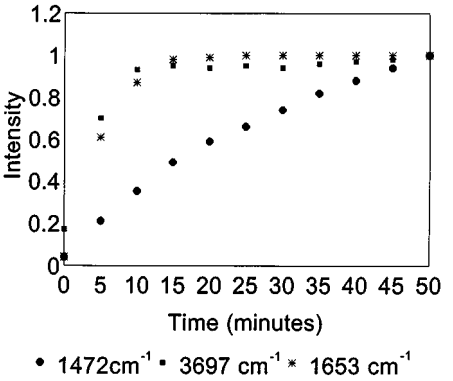

FIG. 9. The normalized intensities of the infrared bands at 1472 cm^{-1} ($v_4(NH_4^+)$), 1653 cm^{-1} ($v_2(NH_3)$), 3697 cm^{-1} (v(OH)) with time during the decomposition of Mg_3N_2.

microscope. At the onset of the reaction when $Mg(OH)_2$ has not been formed to any considerable extent, a very broad and diffuse absorption maximum at ~3000–3700 cm^{-1} represents H_2O and NH_3 species and to a much lesser extent NH_4^+ ions as well. The same is true in the 1600–1700 cm^{-1} wavenumber range, while there are some indications of a very weak absorption maximum at 1400–1480 cm^{-1}, indicative of the presence of NH_4^+ ions. The increase in the concentration of the Mg $(OH)_2$ species, is accompanied by a concomitant increase in the intensity of the $v_4(NH_4^+)$ bands. It is also further evident in Fig. 9 that the intensity of the band centered at 1653 cm^{-1} stabilizes with time while the components of $v_4(NH_4^+)$ continue to grow in intensity, even beyond the point where the intensity of v_{OH} seems to have stabilized. (In the FT-IR measurements under the microscope, the resolution of v_4 into two peaks was not possible.) The decomposition reaction of α-Ca_3N_2 proceeds much faster and could not be followed in the same way as with Mg_3N_2.

As is evident in Fig. 6, $v_4(NH_4^+)$ occurs at 1419 and 1472 cm^{-1} in decomposed Mg_3N_2. The splitting of $v_4(NH_4^+)$ into two components in both of these species confirms a C_{3v} symmetry for the (NH_3–H---O) species. These NH_4^+ bands occur at 1406 and 1459 cm^{-1} in partially decomposed α-Ca_3N_2. $v_4(NH_4^+)$ can also be used as a criterion to probe the strength of hydrogen bonding of the NH_4^+ ion; the higher the wavenumbers at which the components of v_4 occur, the stronger the hydrogen bond. The positions at which v_4 occur show that the hydrogen bonds (NH_4^+---O) are stronger in $Mg(OH)_2$ than in $Ca(OH)_2$. The strength of the hydrogen bond is an indication of the degree of the proton transfer into the NH_3 molecule, which in turn is governed by the polarity of the O–H bond of the proton-donating center. This in turn characterizes Brønsted acidity. $Mg(OH)_2$ therefore has weaker proton-donating centers than $Ca(OH)_2$ or, in other words, demonstrates the fact that the O–H bond is stronger in $Mg(OH)_2$ than in $Ca(OH)_2$. This is obviously due to the existence of weaker hydrogen bonds in pure $Mg(OH)_2$ than in pure $Ca(OH)_2$.

Apart from the intense v_{OH} modes at 3642 and 3697 cm^{-1} in the infrared spectra of $Ca(OH)_2$ and $Mg(OH)_2$, respectively, and at 3620 and 3652 cm^{-1} in their Raman spectra, several weaker features in these wavenumber ranges also occur during the decomposition process. In $Mg(OH)_2$ they occur at 3738, 3712, and 3674 cm^{-1} and can be due to hydrogen-bonded hydroxide species such as H_3N---H–O–Mg--- or even relatively "free" OH ions formed during the reaction.

According to Wilmshurst (17) the wavenumber at which the totally symmetric bending mode v_2 occurs in adsorbed NH_3, can be directly related to the electronegativity of the metal in the compound. The following equation was proposed relating v_2 with the electronegativity of the metal in the compound:

$$v_2^2 \times 10^{-5} = 3.66X + 8.12.$$

It is evident in Fig. 6 that a broad absorption peak occurs at 1080–1100 cm^{-1} in decomposed α-Ca_3N_2, and, although not shown in this figure, the same adsorption peak was observed in some samples of partially decomposed Mg_3N_2 at very much the same position. Using the abovementioned

empirical relationship, the electronegativity X is calculated to be equal to 0.97 eV, which is rather close to the value of 1.1 eV for calcium (17). It is therefore likely that at earlier stages of the decomposition process, Lewis acid centers, or, in other words, unsaturated metal cations, exist at the surface of the solid. This can also explain the fact that the infrared bands at 1641 cm^{-1} in α-Ca_3N_2 and 1653 cm^{-1} in Mg_3N_2 were more intense at the onset of the decomposition reaction before protonation of the adsorbed NH_3 molecules had started.

The intensities of the infrared bands representing the hydroxide, ammonia, and ammonium species in the decomposition product of Mg_3N_2 are graphically represented against time in Fig. 9. It is evident from this figure that the determination of t_0 presents a problem in the case of the formation of $Mg(OH)_2$ and that the measurements were actually started at a value of 0.2 for the normalized infrared intensity. When the sample is exposed to the atmosphere, $Mg(OH)_2$ is formed immediately and the first measurement can only be made after 30–60 s, with the result that an error is introduced. This uncertainty in the determination of t_0 can give rise to serious errors in the determination of the solid state kinetics of this reaction, as has already been pointed out in the decomposition of NH_4VO_3 (18). In other words, if a generalized Avrami–Erofe'ev equation is used to interpret the data, any uncertainty in t_0 will make distinctions between the various rate laws meaningless. The formation of the NH_4^+ ions, which depends on the protonation of adsorbed ammonia molecules, is a much slower reaction but no initial reaction, induction, or acceleratory periods were observed in Fig. 9. This reaction is slow enough to follow with infrared techniques, and the data can be analyzed knowing that the measurements included the start of the reaction. If it is assumed that the intensities of the infrared band at 1472 cm^{-1} represent the amount of product (NH_4^+) present, then the generalized Avrami–Ero'fev equation, $\ln[\ln 1/(1-\chi_p)] = n \ln t + \ln k$, can be used to interpret these results (χ_p = fraction of NH_4^+ present at time t, k is the rate constant, and n is the order of the reaction). The $\ln \cdot \ln$ method of analysis has been applied to all the reaction products viz. $Mg(OH)_2$, NH_3, and NH_4^+ in Fig. 10. Straight lines have been obtained, and in the case of the formation of NH_4^+ ions, n was found to be equal to 1.2 ± 0.05 with a correlation coefficient of 0.995. It is clear from Fig. 10 that with the formation of $Mg(OH)_2$, a straight line is obtained with a slope very similar to that of NH_4^+; however, the slope of this graph was actually found to be much closer to $n = 1$ than to 1.2. The rate-determining step in any solid state reaction will depend on either diffusion, i.e. the transportation of participants to or from a zone where the reaction takes place, the making and breaking of chemical bonds, or on both of these processes. In the decomposition of Mg_3N_2, water vapor has to diffuse to reaction zones within the solid and the NH_3(g) has to diffuse away from these zones to the surface of the solid where it is chemisorbed. The kinetic rate equations based on diffusion mechanisms have been used to interpret the kinetic data obtained on the formation of $Mg(OH)_2$ during the decomposition of Mg_3N_2. The results obtained with the equation describing three-dimensional diffusion, viz. $[1-(1-\alpha)^{1/3}]^2 = kt$ (19) are shown in Fig. 11. A straight line has been obtained with a correlation coefficient of 0.987, which is a reasonable but not particularly good fit to these data, as can also be seen in Fig. 11. k was calculated to be equal to $9.5 \times 10^{-4}\ s^{-1}$. However, it is also evident from Fig. 11 that the data for the formation of the NH_4^+ ions do not fit this equation at all. As mentioned before, the formation of the NH_4^+ ions follows first-order kinetics rather closely and a plot of $-\ln(1-\alpha)$ against t yielded a straight line with a correlation coefficient of 0.989 and $k = 7.18 \times 10^{-4}\ s^{-1}$. Further analysis of the data also made it quite clear that the formation of $Mg(OH)_2$ obeys the abovementioned equation representing three-dimensional diffusion much better than that representing a first-order rate equation.

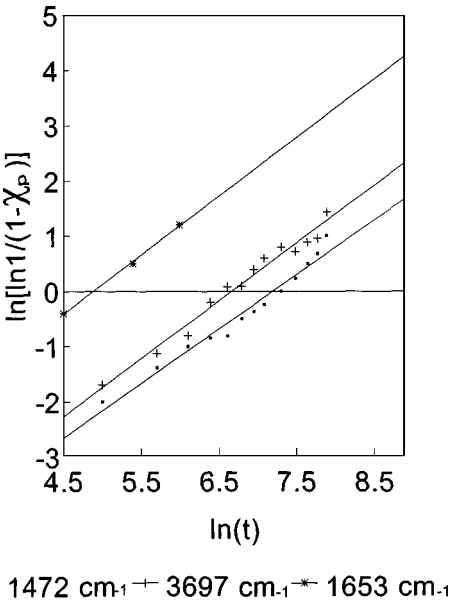

FIG. 10. Plots of $\ln[\ln 1/(1-\chi_p)]$ vs ln plots for the infrared bands of $\nu_4(NH_4^+)$, $\nu_2(NH_3)$, and ν(OH).

It is known that the particle size and particle size distribution of the reactant can influence the kinetics characteristics of thermal decomposition reactions (19). This is particularly true for diffusion-controlled reactions. The average size of the crystals influenced the reaction rate of decomposition of α-Ca_3Na and Mg_3N_2 with the result that in the case of very finely divided particles of Mg_3N_2 (particle size smaller than 0.04 mm), the kinetics of this reaction could not be studied using infrared techniques. However, we were unable to determine any change in the rate law with a decrease in the average particle size and other faster

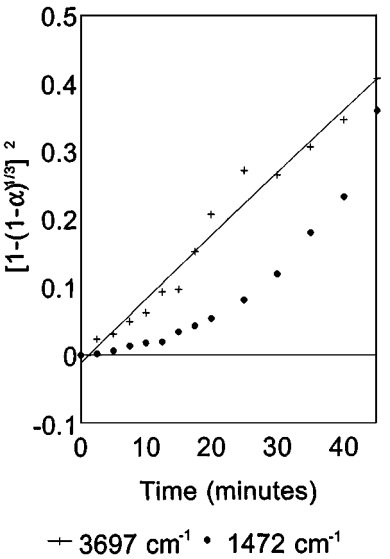

FIG. 11. Obedience of the experimental data of $\nu_4(NH_4^+)$ and $\nu_1(OH^-)$ to the equation representing three-dimensional diffusion, viz. $[1-(1-\alpha)^{1/3}]^2 = kt$.

measuring techniques must be used to establish this beyond any measure of doubt.

ACKNOWLEDGMENTS

Two of the authors (A.M.H. and L.C.P.) thank the University of Pretoria and the Foundation of Research Development (FRD), Pretoria, for financial support.

REFERENCES

1. A. F. Wells, "Inorganic Structural Chemistry", 4th ed., p. 460. Oxford, 1975.
2. M. von Stackelberg and R. Paulus, *Z. Phys. Chem.* **22B,** 305 (1933).
3. Y. Laurent and M. T. le Bihan, *Acta Crystallogr.* **24B,** 494 (1968).
4. P. Höhn, Dissertation, p. 190, Technische Hochschule, Darmstadt, 1993.
5. M. M. Bindal, S. K. Singh, S. K. Singhal, R. K. Nayar, and R. Chopra, *J. Cryst. Growth.* **144,** 97 (1994).
6. H. Hartmann and H. I. Fröhlich, *Z. Anorg. Allg. Chem.* **218,** 190 (1934).
7. Y. Laurent, J. David, and J. Lang, *C.R. Hebd. Seances Acad. Sci.* **259C,** 1132 (1964).
8. R. S. Bradley, D. Murro, and C. Whitfield, *J. Inorg. Nucl. Chem.* **28,** 1803 (1966).
9. J. David, *Bull. Soc. Fr. Mineral. Cristallogr.* **94,** 340 (1971).
10. E. G. Brame Jr., J. L. Margrava, and V. W. Meloche, *J. Inorg. Nucl. Chem.* **5,** 48 (1957).
11. M. Stassen, Dissertation, University of Regensburg, Regensburg, Germany, 1995.
12. W. B. White and V. G. Koramidas, *Spectrochim. Acta* **28A,** 501 (1972).
13. D. M. Adams and D. C. Newton, "Tables for Factor Group and Point Group Analysis." Beckman-RIIc Ltd., Croydon, England.
14. P. Dawson, C. D. Hadfield, and G. R. Wilkinson, *J. Phys. Chem. Solids* **34,** 1217 (1973).
15. A. A. Davydov, "Infrared Spectroscopy of Adsorbed Species on the Surface of Transition Metal Oxides" (C. H. Rochester, Ed.). Wiley, Chichester, UK, 1984.
16. J. K. Wilmhurst, *Can J. Chem.* **38,** 467 (1960).
17. P. W. Atkins, "Physical Chemistry," 3rd ed., p. 823. W. H. Freeman, New York, 1986.
18. D. de Waal, A. M. Heyns, and K.-J. Range, *Mater. Res. Bull.* **25,** 43 (1990).
19. C. H. Bamford and C. F. H. Tipper, Eds. "Reactions in the Solid State," Vol. 22 (Chemical Kinetics). Elsevier, Amsterdam, Netherlands, 1980.